CONF-830909--10

DE84 003311

THE EBT CONCEPT: STATUS, PLANS, AND REACTOR POTENTIAL

D. W. Swain

Fusion Energy Division
Oak Ridge National Laboratory
Oak Ridge, Tennessee 37830

September 1, 1983

To be presented at the

Course and Workshop on Mirror-Based and Field-Reversed Approaches to Magnetic Fusion

Varenna, Italy, September 12-17, 1983

The EBT Concept: Status, Plans, and Reactor Potential*

D. W. Swain

Oak Ridge National Laboratory

Oak Ridge, Tennessee 37830

The ELMO Bumpy Torus (EBT) concept for magnetic confinement fusion has been at the forefront of the "alternate concept" ranks for some number of years. In 1979 a review panel of the U. S. Department of Energy (DOE) recommended that a "proof-of-principle" device be built based upon the EBT concept. This device, called EBT-P, was to be built by McDonnell Douglas Astronautics Company for Oak Ridge National Laboratory (ORNL) and was to cost approximately $86 million. Engineering design work was started on this machine in 1980.

In the past year two things have happened that have caused a reassessment of the overall EBT program. First, financial constraints on the DOE fusion program have caused an indefinite delay in construction of EBT-P, although design work is nearly completed. Second, the present EBT experiment (EBT-S) has produced results in the past year that have caused our estimates of the particle and energy confinement times to decrease. This is due in part to a larger array of sophisticated diagnostics and in part to an improved calculation of the amount of power being deposited in the bulk plasma. The results of these two events have been a reemphasis on understanding the basic physical principles underlying the results in the present experiment and a search for ways in which EBT performance can be improved, either in this present machine or in future generations. This process has led to a series of interesting new ideas, both for improving the present machine operation and for modifying the concept, which may lead to considerably improved plasma performance. This paper will consist of four parts. First, I will describe the basic EBT machine and its operation. Second, I will discuss the experimental results obtained on the present machine and how they relate to neoclassical transport theory. This will include a discussion of the chronology of the estimates of the confinement time and why they have changed. Third, I will briefly discuss some preliminary proposals on how to improve the confinement and operation of EBTs, and fourth I will review some of the potential advantages of EBTs as fusion reactors and the calculations indicating the critical issues.

---

*Research sponsored by the Office of Fusion Energy, U. S. Department of Energy, under contract W-7405-eng-26 with the Union Carbide Corporation.

1. EBT DESCRIPTION AND OPERATION

Machine Description

The ELMO Bumpy Torus (EBT) experiment was constructed in 1973 and first operated using a 30-kW, 18-GHz klystron power source for electron cyclotron heating (ECH). Since then both the magnetic field capability and the power source have been upgraded. This work has culminated in the application of 200 kW of 28-GHz power to EBT from a single gyrotron tube. Results of these experiments through the end of 1982 have been reported extensively.[1,2,3] The EBT device (Fig. 1) consists of 24 simple mirrors joined end to end to form a torus of closed magnetic field lines. The mirror ratio in each cell is 1.9:1. When operated with 18-GHz applied microwave power and a central midplane magnetic field of 5 kG, the device is called EBT-I; when operated with 28-GHz ECH power and a magnetic field of 7.2 kG, the device is referred to as EBT-S. One of the advantages of the EBT concept is that the machine operates in steady state, running for several hours at a time.

Plasma confinement in EBT is the result of the closure of poloidal drift surfaces by particles with drift velocities that are much faster than the vertical drift velocity due to the toroidal field gradient. Magnetohydrodynamic (MHD) stability is provided by the generation of precessing high energy relativistic electrons that form rings encircling the axis in the midplane of each cavity. These rings are observed to form naturally at the second harmonic of the electron cyclotron resonance, as shown in Fig. 2.

The plasma in EBT can be visualized as consisting of three separate components. First, there is the annulus of mirror-trapped relativistic electrons. These have a temperature of approximately 500 keV in EBT-S. The plasma located inside the magnetic field lines that pass through the rings is called the core plasma. It is the component of interest for possible fusion applications. Although the relativistic ring and the core plasma are unstable to MHD perturbations if considered separately, the combined ring-plasma system forms an MHD stable configuration. Ring beta values are typically in the range of 5 to 30%. Outside the magnetic field lines passing through the rings is a volume containing the relatively cold, low density "surface plasma." It is unstable to MHD fluctuations, and such instabilities are observed in that plasma region.

The core plasma and surface plasma are heated by absorption of microwaves at the first and second harmonics of the applied frequency, as shown in Fig. 2. Dimensions and operating parameters of EBT-I and EBT-S are listed in Table 1.

TABLE 1
EBT-S machine parameters

Major radius (m)	1.52
Coil throat radius (m)	0.11
Midplane radius (m)	0.25
Average aspect ratio	9
Number of sectors	24
Mirror ratio	1.9
Peak midplane magnetic field (T)	0.72
Electron ring radius (m)	0.25
Average core plasma radius (m)	0.10
Core plasma aspect ratio	15

Operating Regimes

EBT is usually operated in the steady state, with gas continually fed into one cavity via a feedback control valve to keep the pressure p_0 constant. Pressure is an important variable in EBT operation, because it determines the neutral density, upon which both the core and ring plasma parameters depend sensitively. There are three basic modes of operation of the EBT device. These are illustrated in Fig. 3 as a function of p_0. At higher pressures, there are no hot electron rings and hence no MHD stability. The plasma is relatively dense and cold, and large low frequency fluctuations are present. This regime is called the C-mode. As the pressure is lowered, the rings begin to form. When a critical ring beta of a few percent is reached, the fluctuation level decreases and a warm toroidal core plasma appears, as does a potential well. This regime, called the T-mode, is the regime of normal operation. Upon lowering the presssure still further, the ring beta increases. When the density of the ring electrons becomes approximately equal to one half the core electron density at the ring position, an instability develops, tentatively identified as a hot electron interchange mode. When these fluctuations appear the rings become unstable and the core plasma density becomes very low. This last regime is called the M-mode.

As seen in Fig. 3, for a given applied microwave power (in the example shown, 100 kW), there is a finite range of pressure over which T-mode operation can be obtained. As the applied microwave power is varied, the pressures at which the transitions between the C-mode and T-mode (the C-T transition) and between the T-mode and M-mode (the T-M transition) occur change. The way in which these mode boundaries vary in pressure with microwave power is shown in Fig. 4. We see that for both the C-T and the T-M transitions, the pressure at which these occur increases roughly as $P\mu^{1/2}$. Thus, as applied microwave power is increased, the pressure range over which T-mode operation is obtained is also increased. In the remainder of this paper, I will concentrate on the

properties of the plasma in the T-mode, since this is the mode in which fluctuations are low and confinement is best.

2. RESULTS OF EBT-S EXPERIMENTS

Diagnostics

EBT has a reasonably complete set of conventional plasma diagnostics, including density measurements by a scanning microwave interferometer, potential profile measurements using a heavy ion beam probe, ion temperature measurements via charge-exchange analyzers, and electron temperature measurements via soft x-ray spectroscopy and Thomson scattering. In addition, a novel diagnostic for measurement of electron temperature has been devised by Roger Richards that consists of measuring the relative intensity of the spectroscopic emission of two aluminum ultraviolet spectral lines and obtaining the temperature from their intensity ratio.[4]

The relativistic rings are diagnosed by hard x-ray spectrometers, and their magnetic properties are measured by diamagnetic loops and magnetic pickups. Synchrotron emission is also used as a monitor of the ring behavior.

The density and temperature of atomic neutrals are determined from Balmer-alpha and Lyman-alpha light emissions using a calibrated spectrometer. The density of molecular hydrogen is also measured spectroscopically, as are the density and temperature of impurities. However, in general, the EBT plasma is observed to be quite clean. Z_{eff} is very near to one, and radiation from impurity atoms is an insignificant contributor to power loss.

Measurements

Figure 5 shows the variation in the T-mode of the electron line density $n\ell$, the central density n(0), and the volume-averaged density $<n>$ as a function of gas pressure for 100 kW of microwave power. In this figure the T-M transition occurs at approximately the lowest pressure data point. As can be observed, the ratio of line-averaged density to the central density changes as the pressure is varied, indicating a change in the density profile. Figure 6 shows density profiles obtained from a multichannel microwave interferometer for three different pressures. The ring location is shown by the hatched line. As can be seen, the density profile becomes more peaked as the T-M transition is approached. We can define an effective scale length for the plasma density change by $L_{eff} = n\ell/n(0)$, where n(0) is the central plasma density obtained by Abel inversion. The variation of L_{eff} with microwave power is shown in Fig. 7. For a constant pressure, we observe that the scale length decreases as power is increased (i.e., as the T-M transition is approached). However, if we change the operating pressure proportional to $P\mu^{1/2}$, then the effective scale length remains approximately constant. This is shown in the figure by the curve plotted with triangles, in which L_{eff} is plotted at the

T-M transition, and by the curve shown with squares, which is in the mid-T-mode. In both cases, the operating pressure is varied as $P_\mu^{1/2}$. In later examples we will compare the measured electron temperature and densities with neoclassical theory. In order to make these comparisons more meaningful, we compare different power levels with a constant scale length (i.e., we will generally change the pressure as we change the microwave power in order to keep the plasma profiles constant).

Up until November 1982, the primary diagnostic for electron temperature measurements was the soft x-ray spectroscopy method. The techniques for this measurement have been described in detail in other publications[3] and will not be discussed here. In the next section I will discuss the results of the more recent electron temperature diagnostics (namely, Thomson scattering and the aluminum line ratio method). However, in this section, I will concentrate on the soft x-ray results through 1982, since this is the basis for the earlier confinement time estimates. Figure 8 shows the electron temperature vs pressure for several values of applied microwave power as determined from the soft x-ray diagnostic. We observe that as the pressure is decreased and the T-M transition is approached the temperature increases dramatically for a fixed microwave power. Furthermore, as the microwave power is increased, the electron temperature at a constant gas pressure also increases. Electron temperatures in excess of 1 keV have been measured.

The soft x-ray diagnostic has five separate radial channels, allowing an approximate determination of the dependence of electron temperature on radius. Within the error bars of the measurement, the electron temperature is observed to be flat inside the ring region, as shown in Fig. 9. This result is observed over a wide range of power and pressures in the T-mode.

Figure 10 plots the volume-averaged electron density times the electron temperature as a function of pressure for P_μ = 100 kW. As we have seen before, the electron temperature increases and the density decreases as the pressure is decreased. This results in a fairly weak dependence of the total stored energy on neutral gas pressure. If we assume that the amount of microwave power deposited in the core plasma is relatively insensitive to the neutral pressure, then this implies that confinement time is not a strong function of pressure. This will be discussed further in the next section. In addition to the electron temperature measurements, a cesium heavy ion beam probe is utilized to measure the plasma potential as a function of radius. This instrument, shown in Fig. 11, consists of an ion gun that injects Cs^+ ions with energies from 8 to 36 keV, steering and focusing optics, a detector for the primary ion beam, and a secondary ion detector that detects Cs^{2+} ions. The simplest way to operate this diagnostic is to fix the entrance position and injection angle of the initial beam and, by varying its voltage from 12 to 32 kV, to change the point in space at which the Cs^{2+} ions generated by charge exchange are detected by the secondary detector. This is illustrated in Fig. 12. The curved path indicates the trajectory along which a potential profile can be obtained as the ion accelerating voltage is varied. The value of the potential relative to ground is obtained through

precise measurements of the energy difference between the injected Cs^+ ion and the detected Cs^{2+} ion when it reaches the secondary detector. A potential profile along the curve illustrated is shown to the right of Fig. 12. We see that near the plasma center the potential is negative with respect to ground and grows to a positive value near the ring region. Since the values of electric field are of critical importance to the calculation of neoclassical transport in EBT, these measurements are extremely valuable. Denoting the depth of the potential well as the average of ϕ_{wl} and ϕ_{wr}, we observe that the potential depth is approximately proportional to the measured soft x-ray electron temperature. This is illustrated in Fig. 13, where the ratio of $e\phi/kT_e$ is plotted for the same two constant scale length parametric scans as shown in Fig. 7.

In steady state, the calculation of the energy confinement time for the core plasma can be done using the equation

$$\tau_E = \frac{3/2(<n_e T_e> + <n_i T_i>)V_{core}}{P_{core}}$$

An estimate of $<n_e T_e>$ can be obtained from Fig. 10. The energy stored in the ions is negligible, since the heating due to electron-ion collisions is very small and hence $T_i << T_e$ for this density plasma. One of the largest uncertainties in the calculation of τ_E is the fraction of total applied microwave power P_μ that is deposited in the core. This is denoted by $f = P_{core}/P_\mu$. We have no way of directly measuring this quantity. However, extensive calculations by Batchelor[5] using a ray tracing model for the microwave power propagation and absorption have provided us with estimates of f. Earlier calculations indicated that values of $f \approx 0.12$ (with considerable uncertainties) seemed an appropriate choice. Using this value, and the electron energies shown in Fig. 10, a value for the electron energy confinement time of $\tau_E \approx 3$-4 ms was calculated. In the next section, we will discuss the results of more recent measurements of electron temperature and calculations of power depositions that have caused a downward revision of these estimates.

Recent Experimental Results

Beginning around October 1982, new experimental and theoretical results began to indicate that the confinement time estimates discussed in the preceding section might be an overestimate. The changes came from three sources. First, measurements of electron temperature from the Thomson scattering system and the aluminum line ratio technique began to gain credibility. Second, better data obtained from the 9-channel microwave interferometer provided new information about the density profiles in the plasma. Third, new calculations of the power deposited to the core plasma by the microwaves in EBT-S indicated a substantial increase in the fraction of microwave power deposited. Each of these effects and the consequent changes in confinement time will be discussed below.

Figure 14 shows results from the soft x-ray, aluminum line ratio, and Thomson scattering diagnostics as a function of neutral gas pressure for a fixed microwave power. As can be seen from the figure, there is generally a difference of more than a factor of 2 between the soft x-ray and Thomson scattering results, with the aluminum line ratio data falling somewhere in between. Extensive analysis and review of the diagnostics systems indicate that, although it is conceivable that there are some systematic errors in all systems, it is very unlikely that any change in the diagnostic measurements or analysis will reconcile all these data points to a single curve. The aluminum line ratio diagnostic can have a significant absolute calibration error, relying as it does on the absolute magnitude of two aluminum line intensities. However, the relative temperature determined by the aluminum line ratio technique (i.e., the relative variations in T_e with microwave power and gas pressure) should be very accurate.

If we assume that the individual diagnostics are accurate, there are two possible explanations for the discrepancy in the measured temperatures. First, the temperature profile may be hollow, with a significantly lower value at the center of the plasma than at the edge. Since the soft x-ray and aluminum line ratio temperatures are chord-averaged measurements, both of these will tend to see a mean temperature value, whereas the Thomson scattering apparatus provides a point measurement which historically has been taken at $r = 0$. However, both the temperature profile as determined by the soft x-rays (Fig. 9) and the results from recent radial profiles taken by Thomson scattering (Fig. 15) indicate that the results are not attributable to a hollow profile inside the core plasma. In Fig. 15, the magnetic field was decreased slightly to bring the ring position in to the 8-cm region, which is the maximum extent at which laser Thomson scattering data can be obtained. Similar flat profiles between -4 and +8 cm are obtained with the rings in the normal operating position in which the ring peaks at +12 cm.

A second possibility is that the electron distribution function in EBT is non-Maxwellian and has a substantial high energy tail component. Each of the three diagnostics effectively looks at different energy regions of the distribution function of the electrons. This is shown schematically in Fig. 16. For the temperatures measured by the laser, the population of electrons at energies greater than 300-400 eV is so small that the scattered light is near the limits of the detectability of the system. The best statistical accuracy is obtained from the low energy ends of the spectrum, and that is what largely determines the calculated Thomson scattering electron temperature. In contrast, the soft x-ray measurements are determined by a complicated analysis of the bremsstrahlung obtained from free-free collisions of the plasma electrons. Due to dead zones and windows in the detector system, photons with energies below 400 eV are not counted at all. The detection efficiency of the system gradually increases until ~1000 eV: thus, the soft x-ray diagnostic is looking primarily at the distribution function of electrons with energies of 700 eV and above. Finally, the aluminum line ratio

technique depends on the relative excitation of various ionized aluminum excited states. Calculations indicate that this diagnostic gives approximately equal weight to all electrons between 50 and 1000 eV. Calculations of the response of this diagnostic with the assumption of non-Maxwellian distribution functions indicate that this diagnostic will yield a "temperature" corresponding to approximately the mean energy of the electron distribution function.[6] Thus, the conflicting temperature measurements shown in Fig. 14 could be explained by a roughly bi-Maxwellian distribution function with a high energy tail whose temperature is approximately 2-4 times the temperature of the colder bulk plasma. Preliminary simulation of an EBT plasma by Post et al.[7] using a Fokker-Planck code have produced a non-Maxwellian distribution function with a tail temperature approximately twice the low energy component and approximately equal densities for conditions corresponding to EBT magnetic field, microwave power, and plasma density. Thus, although we cannot definitively say that the distribution function is non-Maxwellian, it is a plausible explanation of our data to date.

Density profile information obtained from the scanning microwave interferometer has allowed us to make better estimates of the volume-averaged density in the plasma. As shown earlier, there are substantial differences between the volume-averaged density and the central density. This effect does not cause a significant change in the central confinement time, but it does cause a decrease of about 25-30% in the calculated volume-averaged confinement time.

Batchelor et al. have carried out extensive calculations of microwave power deposited in various EBT plasmas. Their theories have evolved with time, including more plasma effects and performing the calculations using more realistic geometries. The net result of the changes in the calculations (and the use of more realistic EBT-S geometry) has been to increase the estimated fraction of power absorbed by the plasma core from the previously quoted value $f = 0.12$ to a new estimate of $f = 0.20$.[8] This value is the one which we currently use to calculate τ_E. However, it must be emphasized that the power deposited in the core is a calculated quantity and has not been measured directly.

Table 2 shows the net results of the changes in the electron temperature, volume-averaged electron density, and fraction of power to the core plasma. In this case, we have taken the aluminum line ratio temperature as the best estimate for the mean electron energy. As is illustrated in the table, the value of $<\tau_E>$ calculated with the current results is approximately 1 ms, down from the 3.6-ms value quoted earlier. We should emphasize that due to the uncertainties in the electron energy and the core power, factor of 2 uncertainties in these calculations of τ_E are still likely. These results are illustrated graphically in Fig. 17. The circle labeled (A) indicates the estimates of $<n>T_e$

and P_{core}/P_{μ} used in July 1982 to estimate τ_E. The circle labeled (B) indicates our best estimates of values at present.

TABLE 2
Confinement times for typical EBT-S data

	1982	1983
$P_{\mu\,28\,GHz}$ (kW)	100	100
p_o (10^{-5} Torr)	0.5	0.5
T_e (eV)	600	400
$<n>$ (10^{12} cm^{-3})	1.0	0.7
$P_{core}/P_{\mu\,28\,GHz}$	0.12	0.20
$<\tau_E>$ (ms)	3.6	1.0
$<n\tau_E>$ (10^9 s/cm^3)	3.6	0.7

Comparison of EBT Scaling with Neoclassical Transport Theory

We have seen in the last section that the absolute value of the confinement time is lower than thought previously. However, a more important issue is how the plasma confinement scales as plasma density, temperature and electric field are changed. In particular, does it scale as predicted by neoclassical transport theory, and how well does it agree in absolute magnitude with what one would expect from neoclassical predictions? We will attempt to address those questions in this section.

Colchin et al.[1] has given a review of the predictions of neoclassical scaling for the core electrons when the electrons are in the collisionless regime. These results will be briefly summarized here. Colchin's analysis is for an assumed Maxwellian electron distribution function. However, recent calculations by Hastings et al.[9] indicate that although the value of the diffusion coefficients may change for non-Maxwellian distribution functions the basic parametric dependencies remain the same.

The basic results of neoclassical transport theory may be summarized in two equations:

$$<n>\tau_E \sim T_e^{3/2}(1 + \alpha\, e\phi/kT_e)^2 \qquad (1)$$

$$\tau_E/\tau_p \approx \frac{3}{7}(L_E/L_p). \qquad (2)$$

Here, α is a dimensionless constant (≈ 3 in the EBT-S case) depending on the relative density and electric field scale lengths, and L_E and L_p are the scale lengths for energy and particle changes, respectively.

If, in steady state, we equate the particle source and loss terms and the power source and loss terms and then do a volume average over the core plasma, we obtain the following experimental expressions for the volume averaged particle and energy confinement times:

$$<\tau_p> = 1/<n_o<\sigma v>_i> \quad , \tag{3}$$

$$<\tau_E> = <3/2\, nT_e> V/P_{core} = <3/2\, nT_e> V/fP_\mu \quad , \tag{4}$$

where n_o is the neutral density, $<\sigma v>_i$ is the mean ionization rate for the neutrals , and V is the volume of the core plasma. These last two expressions can be related to the prior two to obtain relationships between experimentally measurable parameters, which should be satisfied if scaling of the plasma confinement is neoclassical. For example, another useful relationship can be obtained by eliminating τ_E from Eqs. (1) and (4):

$$P_\mu \sim <n>^2/T_e^{1/2} \quad , \tag{5}$$

where we have made the approximations (justified by the experimental results) that the electron temperature profile inside the core is approximately flat and that the quantity $e\phi/kT_e$ is constant. In addition, we have assumed that the quantity *f*, the fraction of microwave power deposited to the core, remains constant as plasma parameters are varied. We have no experimental evidence of this, but the theoretical calculations indicate that *f* is relatively insensitive to electron density and temperature over the ranges of our experiment. Finally, for constant scale lengths of energy and particle decay, Eq. (2) becomes

$$\tau_E/\tau_p \approx const \quad . \tag{6}$$

From the experimental results, therefore, if the data points are chosen such that the plasma scale lengths remain constant, experimental verification of the confinement scaling can be made by using the zero-dimensional (0-D) theoretical scaling predictions [Eqs. (5) and (6)]. For the rest of the paper, Eqs. (5) and (6) are referred to as the neoclassical power and particle balance, respectively.

For comparison with the theory, the experimental data used in this scaling study include (i) the line-averaged electron density $n\ell$ and the density profile $n(r)$, (ii) the soft x-ray electron temperature and its radial profile, (iii) the potential well depth, and (iv) the line-averaged H_δ intensity $I_{H_\delta} \sim nn_o\ell<\sigma v>_{exc}$. For typical EBT-S electron temperatures, the excitation rate coefficient is proportional to the ionization rate coefficient $<\sigma v>_i$, which is almost constant. From the scaling point of view, the following experimental observations are worth noting.

(i) For controlled pressure power scans (see Fig. 7), the density scale length can be kept constant. Also, $e\phi/kT_e$ is approximately constant, as shown in Fig. 13.

(ii) As measured by the five-channel soft x-ray diagnostic and Thomson scattering, the electron temperature profile is nearly flat; thus, the temperature scale length is constant up to the hot electron ring.

(iii) The potential profile is approximately parabolic in space, and the electric field scale length is $L_\phi \sim a_{ring}$, where a_{ring} is the radial location of the hot electron ring. Both profile and scale length are independent of operating conditions.

With these experimental observations that the plasma scale lengths and $e\phi/T_e$ are almost constant, the measured values of plasma parameters (n, T_e) having operating points that correspond to the pressures of $p_o \sim P_\mu^{1/2}$ in mid-T mode (case I) and $p_o \approx (p_o)_{TM}$ (case II) can now be used for comparison with the neoclassical power and particle balance predictions.

First, the neoclassical power balance equation is examined. Because the density scale length L_{eff} is a constant, $P_\mu \sim (n\ell)^2/T_e^{1/2}$. Comparison of the experimental value of the right-hand side of this expression with the applied microwave power for case I and case II (Fig. 18) indicates that the electron power balance scales neoclassically within the experimental error bars of the measurements.

To verify the particle balance [Eq. (6)] experimentally, it should be shown that $\tau_E/\tau_p \sim$ constant. By using the definitions of the confinement times and assuming that a constant fraction of the microwave power P_μ is absorbed by the plasma, one can obtain $\tau_E/\tau_p \sim I_{H\delta} T_e/P_\mu$, (assuming negligible or constant molecular ionization contributions), which is a measurable quantity and is plotted as a function of P_μ for the two cases considered here in Fig. 19. Figure 19 indicates that τ_E/τ_p ~ constant, consistent with the prediction of neoclassical scaling.

The electron temperature values used in Figs. 18 and 19 were obtained from the soft x-ray measurements, since more data exist from this diagnostic than the others. However, both the aluminum line ratio and the soft x-ray temperatures show the same qualitative scaling with power and pressure; thus, these results, even in light of the new temperature measurements, still indicate qualitative agreement with neoclassical scaling.

Finally, we address the question of whether the absolute magnitude of the energy confinement time agrees with the value predicted from neoclassical theory. This question is difficult to answer because of the uncertainties of the experimental measurements and the determination of core power. In addition, there are uncertainties in the theory itself (in particular, what the effect of a non-Maxwellian distribution function would be on the calculated transport coefficients). Nevertheless, we have attempted such a comparison, which is shown in Fig. 20.

The expression for the neoclassical confinement time may be written as

$$<\tau_E>_{NC} = k_{NC} T_e^{3/2} (1 + \alpha\, e\phi/kT_e)^2 / <n> \quad , \qquad (7)$$

where k_{NC} is a neoclassical coefficient depending on the geometry of the magnetic field and relative aspect ratio of the torus and α is a quantity that also depends on the geometry and scale lengths of the plasma (see Colchin et al.[1] for a more complete discussion). In our case, $\alpha \approx 3$, so the second term in the parentheses dominates the expression. In addition, 1-D transport simulations have indicated that the electric field near the edge of the plasma is more critical than the potential in determining the average energy confinement time, because as the electric field at the edge increases the transport coefficients in that region decrease substantially over the values near the center. This causes a region of low thermal conductivity on the outside edge that bounds a region of higher thermal conductivity. The result is that net power flow is determined largely by the conductivity of the most resistive layer. Replacing the potential ϕ by the quantity EL_ϕ we obtain

$$<\tau_E>_{NC} = \frac{k_{NC}\, \alpha^2 L_\phi^2 e^2}{k^2} \frac{E^2}{T_e^{1/2} <n>} = \frac{g\, E^2}{T_e^{1/2} <n>} \quad , \qquad (8)$$

where the quantity g is dependent on scale lengths of the plasma system. If we define the quantity c_E as the ratio of the theoretical neoclassical energy confinement time to that measured experimentally, then combining Eqs. (8) and (4) gives us an expression which can be compared with experiment, that is,

$$c_E = <\tau_E>_{NC} / <\tau_E>_{exp} = \left(\frac{2}{3} \frac{g}{V} \right) \frac{P_\mu E^2 f}{<n>^2 T_e^{3/2}} \quad . \qquad (9)$$

Given values of microwave power, electric field, fraction of microwave power coupled to the core, volume-averaged density, and electron temperature, we can calculate c_E. Of these variables, the microwave power and the average electron density are known with reasonably good accuracy. However, the other three variables have considerable error bars. Figure 20 shows contours of constant values of c_E for assumed values of microwave power, volume-averaged electron density, and electric field as functions of T_e and $f (= P_{core}/P_\mu)$. For an electron temperature in the range of 200 to ~550 eV and f in the range 0.1 to 0.22, we observe that c_E can vary from 1 to approximately 10. Our best estimates for T_e and f, with appropriate error bars ($T_e \simeq 400$ eV and $f \simeq 0.2$), yield values of c_E = 2-4. That is, the confinement time measured experimentally appears to be one-half to one-fourth the value calculated from neoclassical theory.

In summarizing the results of the recent confinement studies, experimentally measured confinement times on the order of 1 ms are observed in EBT-S, with factor of 2 error bars. However, the scaling of the confinement with plasma parameters such as electron density and temperature

appears to be qualitatively the same as predicted by neoclassical theory. The absolute energy loss rate appears to be 2-4 times the predicted neoclassical value.

3. IMPROVEMENTS TO THE EBT CONCEPT

The results of the preceding section indicate that although confinement in the present EBT experiments scales approximately neoclassically the absolute value of confinement time for any given set of parameters is 2-4 times smaller than that predicted by neoclassical theory. These results have generated an increased interest in studying EBT-like devices (i.e., closed field line devices with bumpy magnetic fields and electron rings) in which neoclassical confinement is predicted to be substantially better than in the present simple, closed toroidal configurations. The recent United States-Japan workshop on advanced bumpy torus concepts, held in California July 11-13, 1983, was attended by about 60 participants. The purpose of the workshop was to provide a forum for presentation and discussion of recent developments on advanced bumpy torus concepts. In order to give a flavor for some of the ideas being considered, and with the kind permission of some of the authors of the 25 papers presented, I will review briefly in this section some of the criteria by which these new concepts were being evaluated and will describe three of the new concepts presented.

The technical coverage in the workshop was very broad. Many of the concepts were based on the present closed field line EBT-like system but with a different magnetic field coil geometry. Others included some features not normally associated with EBTs, such as rotational transform to provide better confinement and/or stability. It should be emphasized that most of these concepts have undergone very preliminary evaluation; in particular, most of the analyses have been done for the vacuum magnetic field cases only, and details of equilibrium and stability are quite incomplete at this time. Therefore, this is a progress report rather than a completed set of investigations.

Most of the analyses carried out so far on these advanced concepts consist of looking at single particle orbits and calculating diffusion coefficients based upon the single particle results. In any bumpy torus device, particles can be divided into two classes: trapped particles that bounce back and forth in the region between any two adjacent coils and passing particles that traverse all the way around the torus. In any toroidal device, there is a vertical drift caused by the gradient in the major radius direction of the applied magnetic field. In EBT, superimposed on this vertical drift is a second drift in the poloidal direction caused by the gradient in minor radius due to the "bumps" in B. The superposition of these two drifts results in closed particle orbits that are generally shifted inward from the center of the machine. The relative amount of shift (and hence the size of the orbit that can be contained in the machine without hitting the wall) depends on the pitch angle in velocity space of the particles. This effect is shown in Fig. 21(a) for the standard EBT-S geometry, where the drift

orbits of completely trapped particles (i.e., with $v_{\parallel} = 0$) and perfectly passing particles (i.e., $v_{\parallel} = v$) are shown in the cavity midplane. As can be seen in the figure, the area enclosed by the passing particle orbit is considerably smaller than that enclosed by the trapped particle orbit. Figure 21(b) shows $F(v_{\parallel}/v) = A(v_{\parallel}/v)/A(v_{\parallel} = 0)$, the ratio of the area enclosed by the largest contained orbit of a particle with a given pitch angle relative to a particle with $v_{\parallel} = 0$, as a function of $v_{\parallel}/v$. This figure indicates that for $v_{\parallel}/v$ in the range 0.7-0.8 the area of confined particle orbits is either very small or nonexistent in the present EBT device. This curve of fractional area vs $v_{\parallel}/v$ is one of the figures of merit by which proposed new concepts can be judged: their fractional area should be substantially better than EBT-S. In addition, an average neoclassical diffusion coefficient can be computed for a given T_e and n, since the mean step size of a collision can be determined from this curve. Thus, a second criterion (figure of merit) that has been used is the ratio of the calculated neoclassical diffusion coefficients for the proposed improved geometries relative to those for EBT-S. In some cases, these diffusion coefficients show an improvement of better than a factor of 10 in confinement relative to the EBT-S case.

Closed Magnetic Field Line Improvement Examples

Figure 22 shows a plan view of ELMO Bumpy Square (EBS) proposed by Owen et al.[10] of ORNL. ELMO Bumpy Square is designed as a substantial upgrade of the present EBT-S device. It uses the 24 circular magnetic field coils from EBT-S to form four straight sections, as shown in the figure. These are connected via high field corner regions. The field in the corner is approximately twice the field in the mirror throat regions of the straight sections. The advantage of this proposed geometry is that the drift surfaces are much more nearly centered on the geometric axis of the machine than in the standard torus, because toroidal drift occurs only in the four relatively short curved regions, and the high field value in those regions minimizes those drifts relative to the poloidal precession. Figure 23(a) shows drift orbits for $v_{\parallel} = v$ and $v_{\parallel} = 0$ for EBS, while Fig. 23(b) indicates $F(v_{\parallel}/v)$ for this device. As can be seen from the figures, the orbits are much more closely centered, and there is less dispersion in the drift orbits of trapped and passing particles relative to the conventional EBT. Diffusion coefficients for this geometry have been calculated by Owen and have values approximately an order of magnitude below those calculated using similar techniques for EBT-S.

This concept maintains many of the potential advantages of the EBT: it is of relatively simple modular construction, it uses rings for MHD stability, and it can be run steady state. Magnet construction for the throat region looks feasible from a preliminary engineering study. A significant open question for this device (and, indeed, for most of the configurations presented) is the overall

stability of the device. The effect of the high magnetic field corners on MHD stability has not been evaluated in detail yet. This work is under way at present.

Another closed field line device discussed at the workshop was by R. L. Miller et al.[11] of Applied Microwave Plasma Concepts. A plan view of the magnetic configuration of this device is shown in Figure 24. This device is denoted as theELMO Bumpy Torus/Enhanced Confinement (EBTEC) configuration. This concept has magnetic field coils arranged in a simple circular torus; however, instead of being circular,the coils are racetrack shaped with a 2:1 elongation. As shown in the figure, the elongated coils are positioned alternately with their long axis in the horizontal and the vertical planes. In addition, there is a considerable shift in major radius of the center of the coils, with those oriented in the horizontal direction being moved inward relative to those with a vertical orientation. As in the preceding example, the result of this modification to the magnetics is the improvement of the orbits in the device relative to EBT-S. Figure 25(a) shows the fully trapped and passing particle orbits for an EBTEC device with a major radius R = 500 cm. Figure 25(b) indicates the fractional area F vs $v_{\parallel}/v$ for this configuration. As in the preceding case, the improvement in fractional area is substantial over the conventional EBT case.

Closed Flux Surface Example

A second class of configurations considered at the workshop was one in which bumpy magnetic fields with rings were used to achieve stability and rotational transform was introduced to improve confinement. One such approach has been proposed and analyzed by Pipkins et al.[12] at McDonnell Douglas Astronautics Company. A picture of their device, called the "Twisted Racetrack Torus" (TRT), is shown in Fig. 26. It is composed of straight mirror sections with approximately 2:1 mirror ratios that are connected by curved solenoids with approximately constant magnetic fields on-axis in the solenoid region. The straight sections contain rings to provide stability as in EBT. The curved sections do not contain rings and have an on-axis field approximately equal to the magnetic field in the coil throats of the straight sections.

The straight and curved sections are connected in a figure-eight pattern as shown in the figure. This introduces rotational transform so the field lines no longer close and flux surfaces are produced. For the device shown, the magnetic geometry results in a q = 2.2 device, where q is the number of times a magnetic field line must transit the device to experience a 360° rotation around the minor axis.

Calculations of confinement time have been made for the TRT device, based on 0-D neoclassical theory. These results are shown in Fig. 27. The size of the TRT shown here has been chosen to have a perimeter approximately equivalent to the EBT-P device[13] and approximately the same minor radius. Details of the transport calculations are given in Pipkins' paper. As can be seen from the

figure, the calculated confinement times for the TRT are over a factor of 10 improved over the comparable EBT-P confinement times for electron temperatures ≥ 1 keV.

Summary of Concept Improvements

There are many devices now under theoretical investigation that might have improved confinement and/or stability properties relative to a classic EBT device. I have only given a very cursory look at three examples in this paper. There are still significant questions to be answered, such as stability of the devices to various modes and properties of each configuration as plasma beta is increased. This work is now under way. In the next six months, criteria for selecting the most promising improved concept will be established by a concept improvement committee headed by N. A. Uckan, and across-the- board theoretical comparisons of the various concepts will be made. Based on the results of the theoretical evaluations and on the achievement of an improved understanding of the present EBT-S operation, we hope to propose a new device to DOE that will have approximately the same size as the present EBT-S device but that will allow us to test experimentally the most promising of the new, improved concepts. Since several of the concepts proposed exhibit calculated confinement time improvements on the order of a factor of 10 over the present circular EBT devices, significantly improved operation is anticipated .

4. REACTOR POTENTIAL

Historically, there have been several aspects of the EBT concept that made it particularly attractive as a reactor. They are the large aspect ratio, the simple magnetics resulting in an inherently modular design, and the steady-state operation. There have been several studies of the reactor potential for an EBT, which have considered many aspects of the design, construction, stability, and power balance of an EBT reactor. In this section, I will discuss very briefly the critical issues for an EBT reactor and present some results for an EBT reactor design as given by Uckan et al.[14]

The recent reactor calculations were done based on neoclassical EBT scaling; that is, their scaling would predict confinement times somewhat better than those presently observed in EBT-S. However, as described in the last section, there are several concepts for improving the confinement of an EBT-like device, often a factor of >10. Therefore, I will present the results of a reactor configuration for a conventional circular EBT device, assuming standard neoclassical scaling. However, to achieve parameters such as those predicted for such a reactor, it may be necessary to change from the standard configuration to one of the improved concepts.

Critical Issues

The main issues in designing an EBT reactor are similar to those for the other magnetic confinement devices: confinement, including the scaling of confinement time with temperature and density; the maximum beta value which can be achieved in a reactor, which determines the magnetic field necessary for operation; the minimum size necessary for economical power production, which determines the overall cost and complexity of the device; impurity production and control; engineering design, including first wall material and design; heating sources; and economics of operation. In addition to these, the EBT concept has other considerations: namely, the temperature and density of the relativistic electron rings necessary for stability, and the effect of ring losses on the reactor power balance.

In this paper, I will not discuss the impurity problem or the specific engineering design of the reactor. Impurities in the present experiment do not seem to be a significant problem, since they are shielded out of the core plasma, and impurity effects and radiation are negligible in the present experiment. The engineering aspects of an EBT reactor design have been studied in some detail.[15] Compared to other devices, such as the tokamak, the large aspect ratio and the inherent modularity of the EBT device make it relatively simple to design a reactor based on the circular EBT concept.

The critical questions concerning electron rings are the ring beta necessary for stability and the ring thickness. In EBT, the stability requirements of the core plasma and the energetic rings are closely coupled, and their interaction defines the stable operating limits of both plasmas and determines the core beta (β_c) limits, as well as the allowable upper and lower limits of the ratio of the core to the hot plasma densities (n_c/n_h). Much theoretical research has been done in the last several years on the stability boundaries for the coupled core-ring system. The reactor study of Uckan and Santoro[14] differs from earlier ones primarily by including the theoretical stability criteria [particularly the Lee-van Dam-Nelson (LVN) limit] and coupling the output of the stability results to the ring power requirements.

The results of a stability boundary calculation are shown in Fig. 28. The modes that have been considered in this analysis are the core interchange, hot electron interchange, and interacting ring-core interchange (LVN) modes. Typically, these modes impose restrictions on the upper and lower limits of n_c/n_h, an upper limit on β_c, and a lower limit on β_h. The magnitude of these restrictions are determined by geometrical features of the reactor design and other plasma parameters, such as the ring thickness Δ, the radius of curvature R_c (local and/or field line averaged), the dimensionless ratio of the curvature drift frequency to the ion cyclotron frequency, plasma anisotropy, etc. Also shown in the figure is a region of high beta, high temperature operation for the rings in which there is no net reactor power production because the ring losses due to synchrotron radiation are excessively high.

Within the constraints that the reactor parameters must lie within the operating window shown in Fig. 28 for stability, a favorable reactor design can be obtained that has satisfactory values for both the recirculated power fraction and the total fusion power produced.

Effects of Core Presssure Profile

The economic viability of an EBT reactor will improve noticeably if the average core beta significantly exceeds 5%. The radial profiles of the core plasma pressure are found to play an important role in both fusion and ring power balance. A limitation on the core plasma beta at the ring location is given by

$$\beta_c(r_{ring}) < \frac{2\Delta}{R_c}(1 + p_{\parallel h}/p_{\perp h}) \quad . \tag{10}$$

Because the magnetic field in the center and coil throat regions of the plasma is significantly higher than that at the ring location, a relatively flat core pressure profile will result in a volume averaged beta value $<\beta_c>$ significantly less than the critical value at the ring given by Eq. (10):

$$<\beta_c> \leq \beta_c(r_{ring})/4 \quad . \tag{11}$$

However, if the pressure profile is peaked at the plasma center, then $<\beta_c>$ can be comparable to the local critical core beta at the ring,

$$<\beta_c> \approx (0.5 - 1.0)\,\beta_c(r_{ring}) \quad . \tag{12}$$

One and one-half dimensional (1-1/2 D) transport analysis (discussed in the next section) indicates that it should be possible to maintain pressure gradients in the core plasma, thus improving the value of the volume-averaged core beta and allowing values in the 10-15% range.

Confinement Scaling

As we saw in Sect. 2, the EBT neoclassical electron transport scaling appears to be given by Eq. (7). In EBT-S, ion transport is dominated by charge exchange losses, so it is difficult to make comparisons between any theoretical ion losses and experimental observations in the present device. However, scaling laws governing ion behavior will be important in a reactor. At present, the ion transport principally determines the radial electric field needed to maintain ambipolarity. In the experiments the radial electric field $E_r < 0$; however, $E_r > 0$ is also possible in theory, which could yield enhanced ion confinement. In a 0-D analysis with $E_r < 0$, it is observed that large devices with aspect ratios $A > 20$ are required for ignition. However, recent analyses that have been done with the 1-1/2 D transport simulation code provide an important new insight in the confinement scaling of EBT in going from the present EBT-S experiment to a reactor. It is observed that from the EBT-S to EBT-R sequence, profile effects near the outer edge of the hot electron ring lead to enhanced confinement beyond the simple scaling obtained from Eq. (7), which omits these profile effects. This is illustrated in Fig. 29, which plots the values $n\tau_E$ vs a dimensionless collisionality parameter

predicted by transport code runs for various devices. The dashed curves represent the values of $n\tau$ calculated from the 0-D scaling of Eq. (7), whereas the solid curves represent the results from the profile calculations. For the reactor case (denoted by EBT-R), an enhancement of a factor of 4 in confinement over the 0-D scaling is predicted, for a given value of collisionality.

Summary of Reactor Calculations

Uckan et al. have carried out systematic parametric studies of reactor properties using a systems reactor code developed by Santoro.[16] Considered in that code are the coupling of the ring and core plasma, the consistent treatment of stability and power balance, and preliminary cost calculations. A reactor operating space obtained from the systems code is similar to that shown in Fig. 28. Within that operating window, a representative set of reactor parameters is given in Table 3. Similar values for reactor parameters have been obtained by other authors also.[15]

TABLE 3
Representative EBT Reactor Parameters

Thermal power [MW(t)]	5000
Net electric power [MW(e)]	
Electron ring	1550
Ion ring	1650
Major radius (m)	38
Average plasma radius (m)	1.5
Number of sectors	34
Average magnetic field (T)	4 T
Neutron wall loading (MW/m^2)	1.4
Average core density (m^{-3})	8×10^{19}
Average core temperature (keV)	25
Core/ring beta (%)	10/15
Ring temperature (MeV)	2
Ring power losses (MW)	
Electron ring	60
Ion ring	5

Reactor Summary

The extrapolation of the present EBT results to a reactor has been carrried out based largely on the assumption of neoclassical scaling and the validity of the stability calculations. The theoretical estimates indicate that it may be possible to build an EBT concept reactor with excellent engineering properties and with satisfactory confinement properties if the scaling and stability scaling calculations are correct. It indicates the possibility of quite interesting reactor performance. The next-generation devices for EBT should help to address some of the questions involving the confinement scaling necessary for extrapolation to a reactor and will likely test one or more of the new improved concept ideas.

ACKNOWLEDGMENTS

Many people have contributed to the material presented in this paper. I wish to thank in particular R. J. Colchin and the EBT group for the experimental data; L. W. Owen et al. (ORNL) for the EBS results and Figs. 22 and 23; R. L. Miller and his cohorts at AMPC for the EBTEC results and Figs. 24 and 25; and W. B. Ard and his colleagues at MDAC for the TRT results and Figs. 26 and 27. Finally, the section on reactors is a much abbreviated version of a paper by Uckan and Santoro (Ref. 14).

REFERENCES

1. R. J. Colchin, T. Uckan, F. W. Baity, L. A. Berry, F. M. Bieniosek, L. Bighel, W. A. Davis, E. Dullni, H. O. Eason, J. C. Glowienka, G. A. Hallock, G. R. Haste, D. L. Hillis, A. Komori, T. L. Owens, R. K. Richards, L. Solensten, T. L. White, J. B. Wilgen, Plasma Phys. 25, 597 (1983), and references therein.

2. N. A. Uckan and EBT Group, Plasma Phys. 25, 129 (1983), and references therein.

3. D. L. Hillis, G. R. Haste, L. A. Berry, Phys. Fluids 26, 820 (1983).

4. R. K. Richards, Bull. Am. Phys. Soc. 28, 928 (1983).

5. D B. Batchelor, Nucl. Fusion 21, 1615 (1981).

6. R. K. Richards (private communication).

7. R. S. Post (private communication).

8. D. B. Batchelor, R. C. Goldfinger, D. A. Rasmussen, D. W. Swain, in *Proc. of the Advanced Bumpy Torus Concepts Workshop*, Rancho de Santa Fe, California, 1983 (Oak Ridge National Laboratory CONF-830758, 1983), p.414; D. B. Batchelor, D. A. Rasmussen, Oak Ridge National Laboratory Report ORNL/TM-8770 (to be published).

9. D. E. Hastings (private communication).

10. L. W. Owen, D. K. Lee, C. L. Hedrick, in *Proc. of the Advanced Bumpy Torus Concepts Workshop*, Rancho de Santa Fe, California, 1983 (Oak Ridge National Laboratory CONF-830758, 1983), p. 55.

11. R. L. Miller, R. A. Dandl, G. E. Guest, *ibid.*, p. 37.

12. J. F. Pipkins, R. J. Schmitt, W. B. Ard, R. J. Kashuba, F. M. Bieniosek, *ibid.*, p. 99; R. J DeBellis, H. F. Imster, J. L. Conlee, R. J. Dannenmuller, C. F. Dillow, T. J. Poteat, R. J. Schmitt, *ibid.*, p. 117.

13. A. L. Boch, Oak Ridge National Laboratory Report ORNL/TM-7066, Oct. 1979; J. C. Glowienka, in *Proc. of the 12th Symposium on Fusion Technology*, Julich, Germany, 1982 (to be published).

14. N. A. Uckan, R. T. Santoro, in *Proc. of the Fifth Topical Meeting on Tech. of Fusion Energy*, Knoxville, Tennessee, 1983 (to be published in Nuclear Technology/Fusion), and references therein.

15. C. G. Bathke, D. J. Dudziak, R. A. Krakowski et al., Los Alamos National Laboratory Report LA-8882-MS, Aug. 1981.

16. R. T. Santoro, N. A. Uckan, J. M. Barnes, in *Proc. of the Fifth Topical Meeting on Fusion Energy*, Knoxville, Tennessee, 1983 (to be published in Nuclear Technology/Fusion), and references therein.

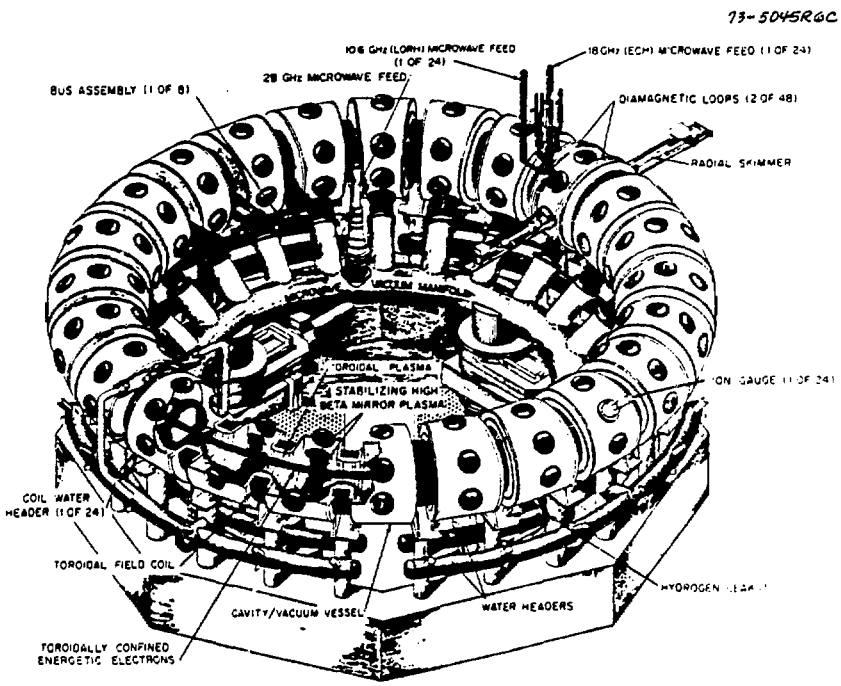

Fig. 1. ELMO Bumpy Torus (EBT).

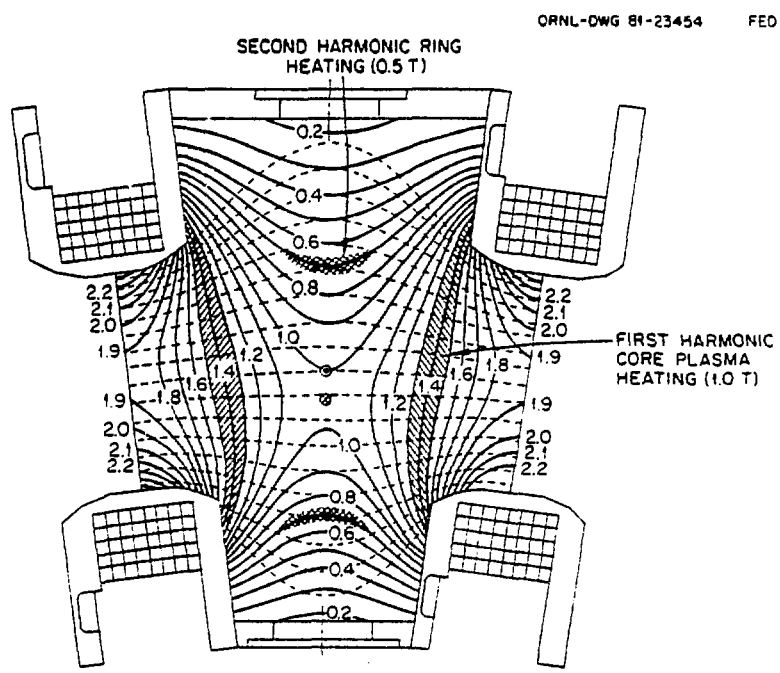

Fig. 2. Horizontal cut of an EBT cavity, showing magnetic field lines (dashed curves), and contours of constant |B| normalized to the center of the midplane.

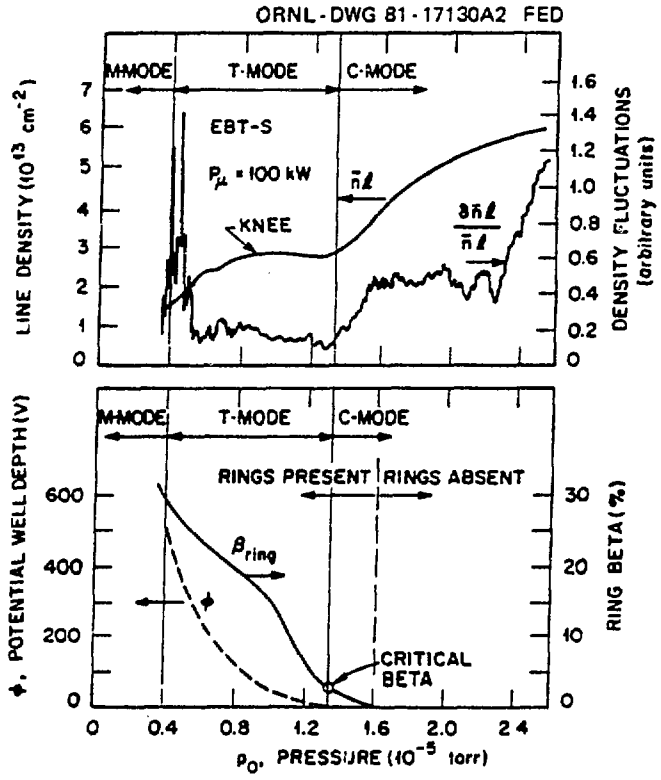

Fig. 3. Variation of plasma parameters as a function of pressure. The line-averaged electron density $n\ell$, the normalized density fluctuations, the average ring beta (β_{ring}), and the potential well depth ϕ are plotted as a function of neutral gas pressure.

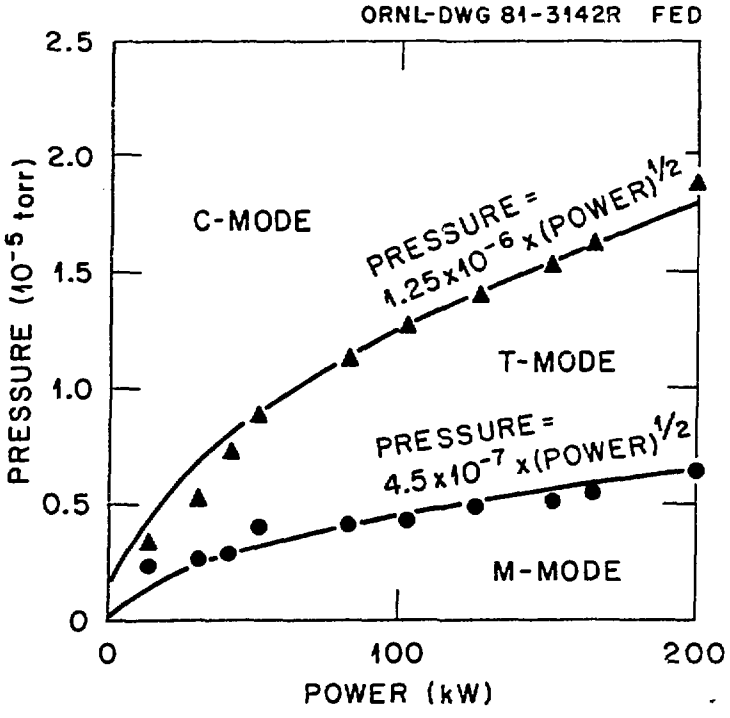

Fig. 4. Mode transistion boundaries as a function of pressure and power. Empirical fits to the data point are shown as solid lines.

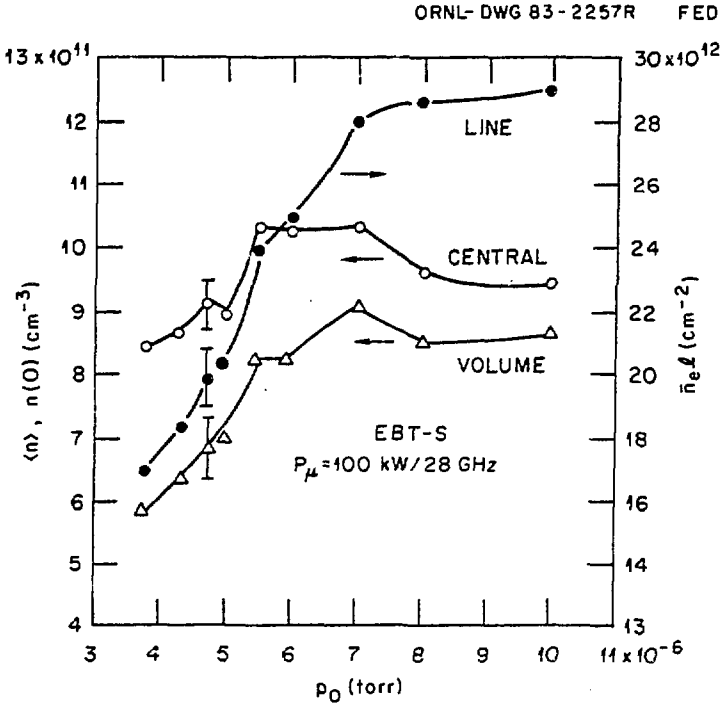

Fig. 5. Variation of line integral electron density $n\ell$, central electron density n(0), and volume-averaged electron density $\langle n \rangle$. P_μ = 100 kW.

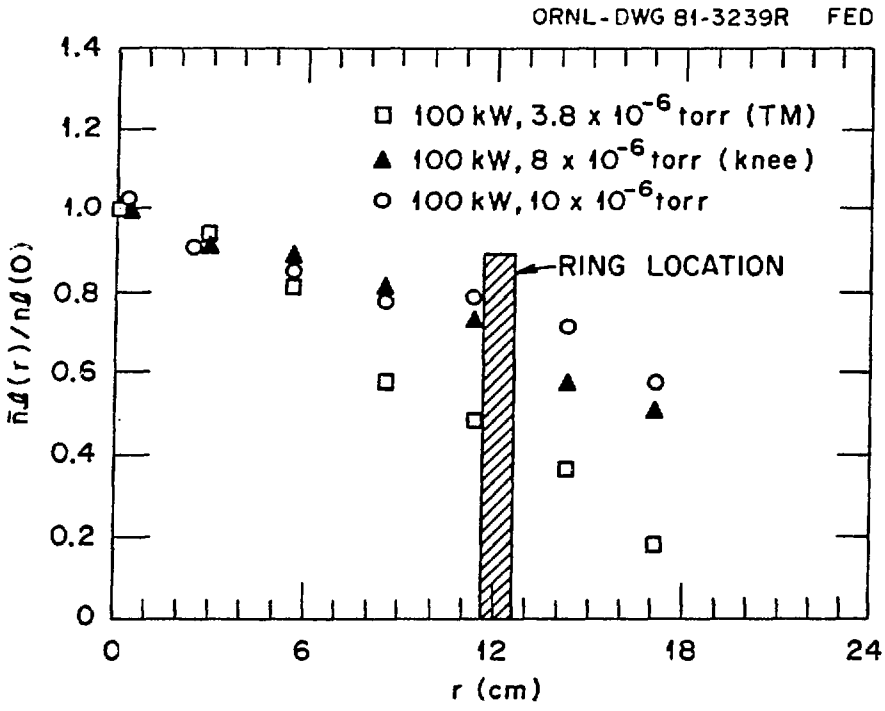

Fig. 6. Line integral densities at several radii for three different pressures. These data were obtained from a multichannel microwave interferometer.

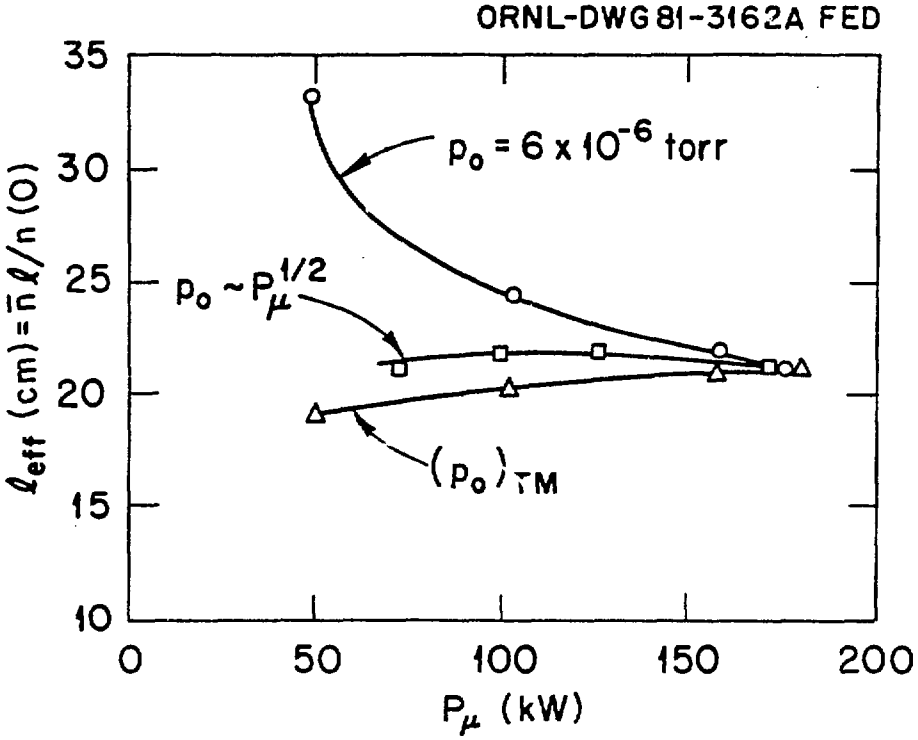

Fig. 7. Effective density scale length L_{eff} as a function of microwave power. For a constant pressure L_{eff} decreases with increasing power, but is almost constant for a controlled power pressure combination.

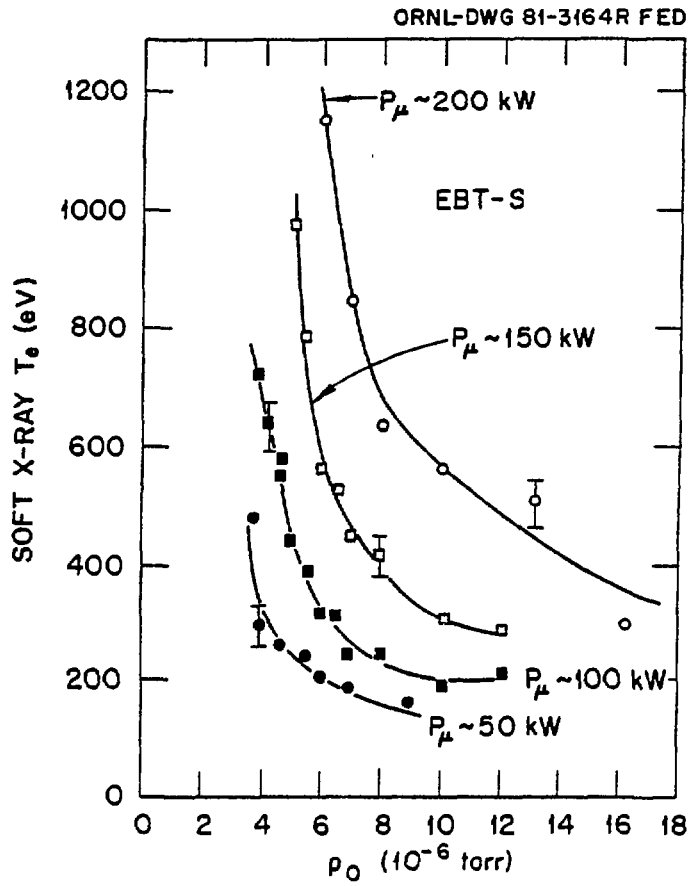

Fig. 8. Electron temperature (as determined from the soft x-ray diagnostic) as a function of pressure for different applied 28-GHz power levels.

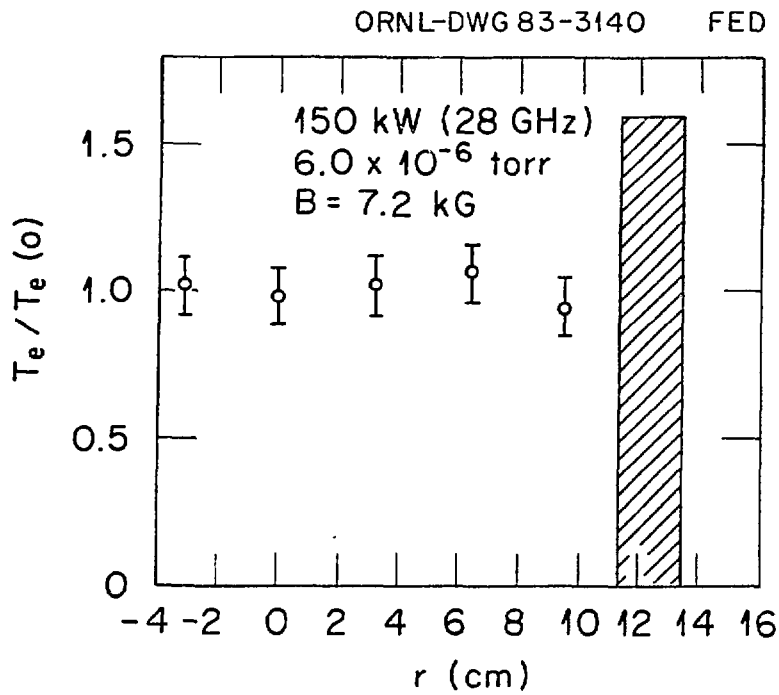

Fig. 9. Relative electron temperature profile determined from the soft x-ray measurements. The ring region is shown by the hatched area.

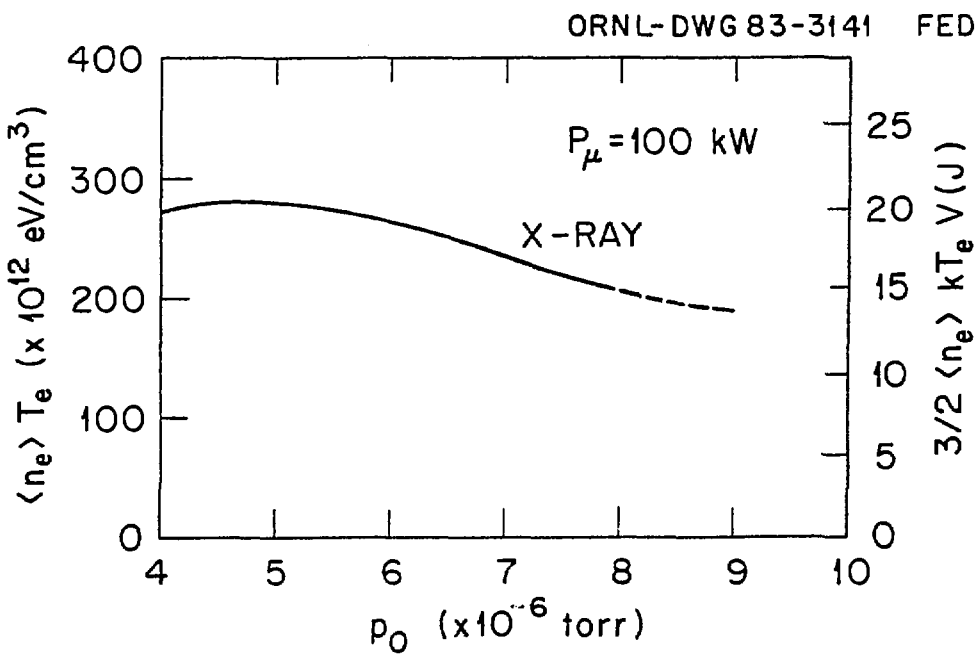

Fig. 10. Volume-averaged electron energy density, and total plasma core energy vs neutral pressure. Temperature is determined from the soft x-ray measurements; volume-averaged density, from the multichannel microwave interferometer.

ORNL-DWG 83-3164 FED

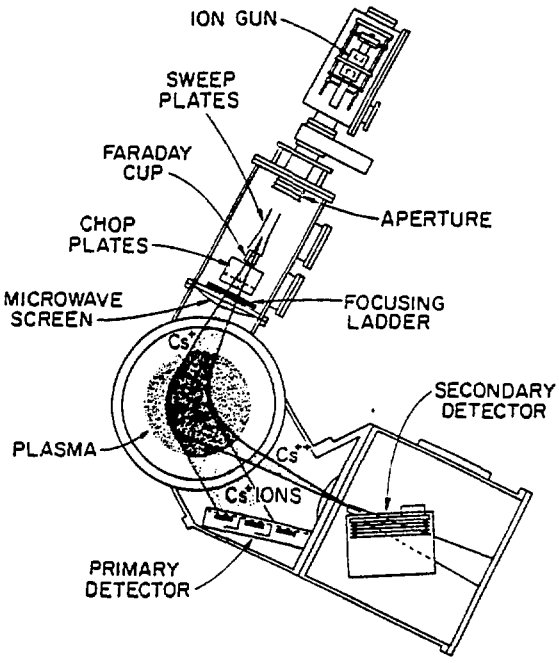

Fig. 11. Schematic diagram of the heavy ion beam probe accelerator and detection system.

ORNL-DWG 83-3165 FED

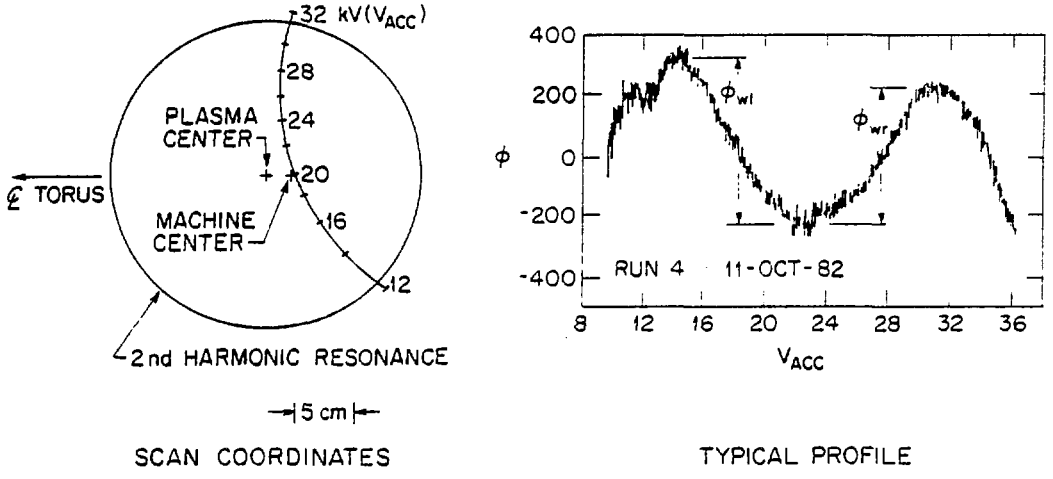

Fig. 12. Left: Curve along which potential is measured as a function of heavy ion beam probe acceleration voltage (V_{acc}). Right: plasma potential vs V_{acc} along the trajectory shown for P_μ = 100 kW in mid-T mode.

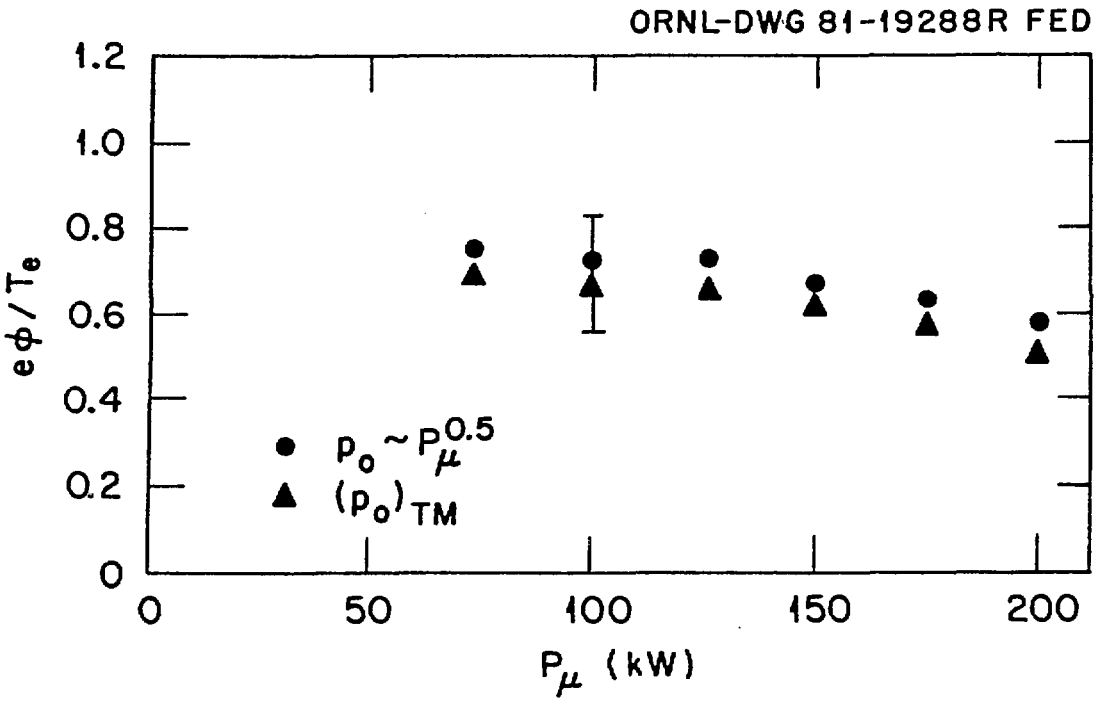

Fig. 13. Ratio of well depth to electron temperature vs microwave power for two cases corresponding to p_0 proportional to $P_\mu^{1/2}$.

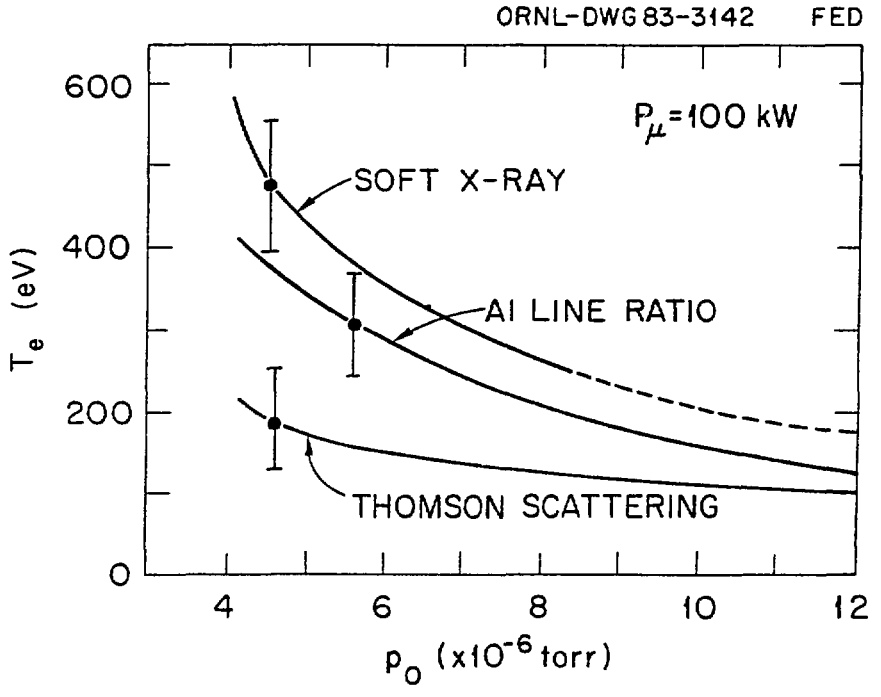

Fig. 14. Electron temperature vs neutral pressure as measured by soft x-ray, aluminum line ratio, and Thomson scattering techniques for P_μ = 100-125 kW.

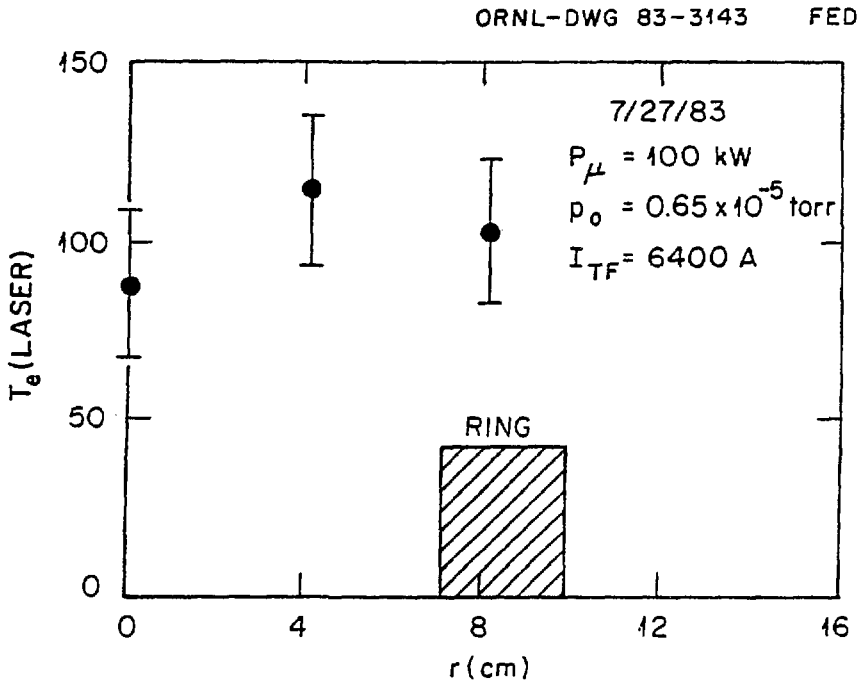

Fig. 15. Partial Thomson scattering temperature profile for mid-T mode and P_μ = 100 kW. The toroidal field was lowered for this run to bring the ring region into the viewing area of the Thomson scattering system.

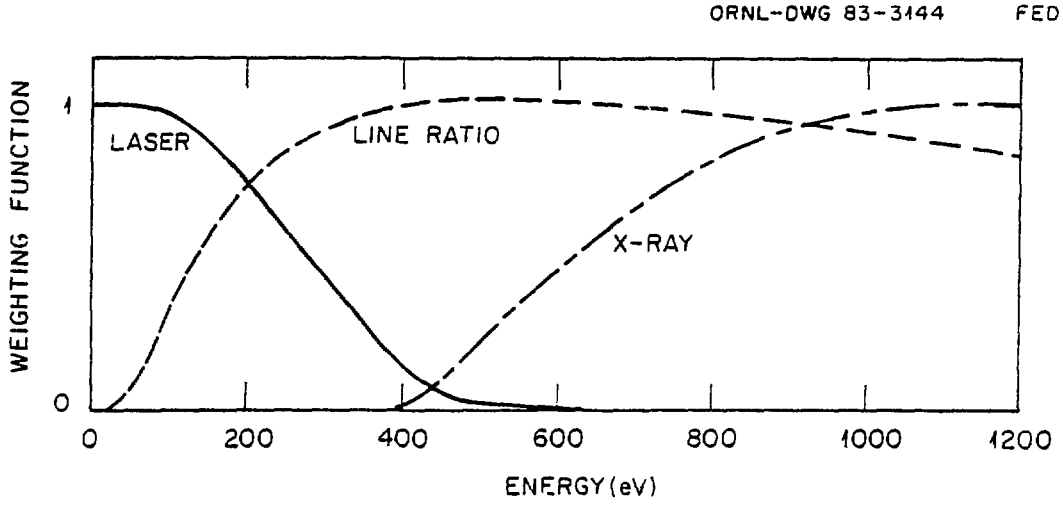

Fig. 16. Schematic indication of the relative importance of different energy regions in determining the electron "temperature" measured by the three temperature diagnostics.

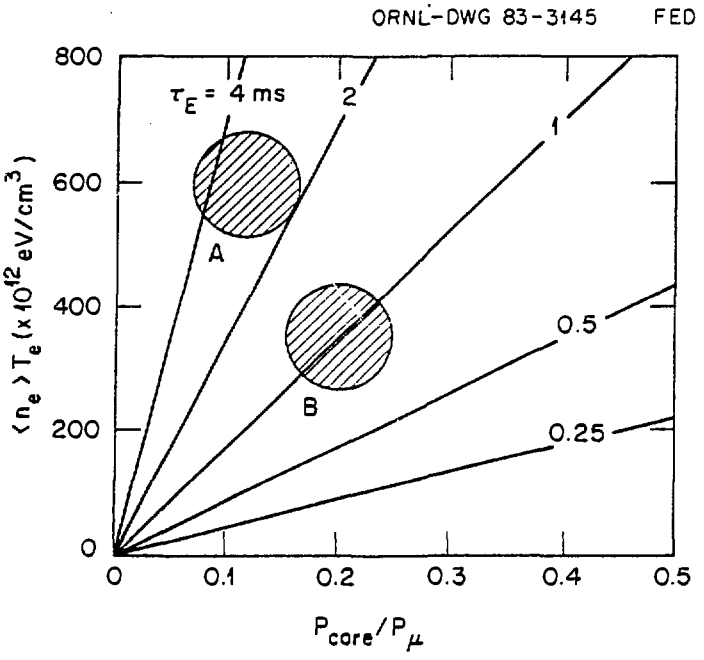

Fig. 17. Volume-averaged electron energy density vs P_{core}/P_μ. The straight lines are contours of constant electron energy confinement time. Shaded circle A indicates the 1982 τ_E estimate. The circle labelled B indicates the current estimate.

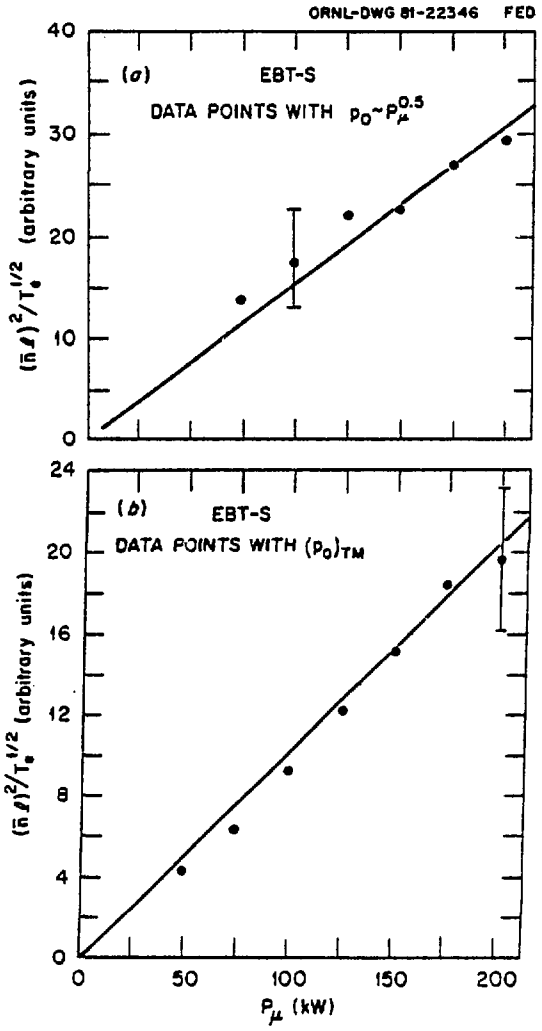

Fig. 18. The relationship between microwave power and electron line density and temperature, indicating that for constant scale length cases (i.e., $p_0 \propto P_\mu^{1/2}$) the power balance scaling is consistent with neoclassical predictions.

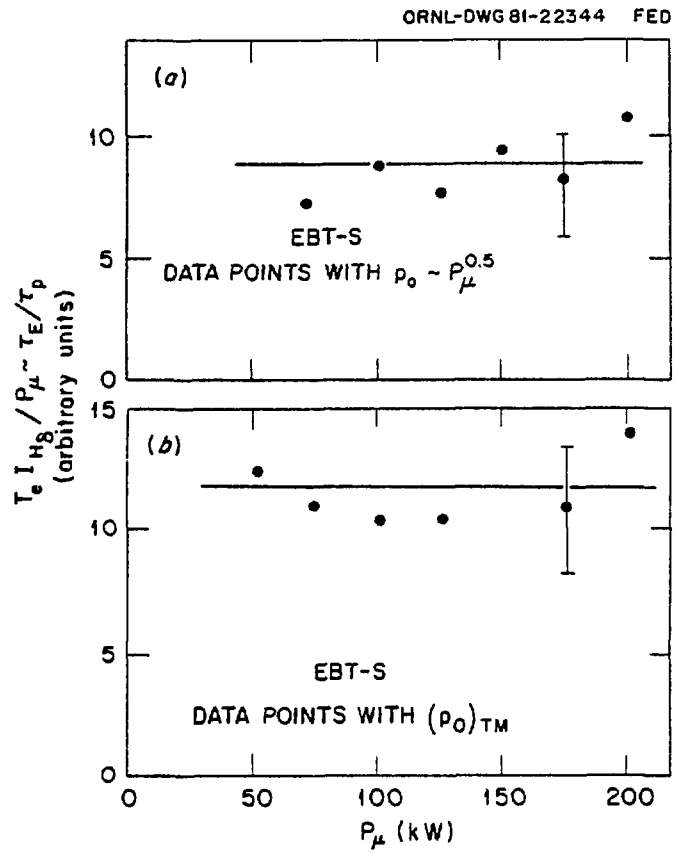

Fig. 19. Ratio τ_E/τ_p, which is experimentally observable through $T_e I_{H\delta}/P\mu$, is consistent with neoclassical scaling for constant scale lengths and constant $e\phi/kT_e$.

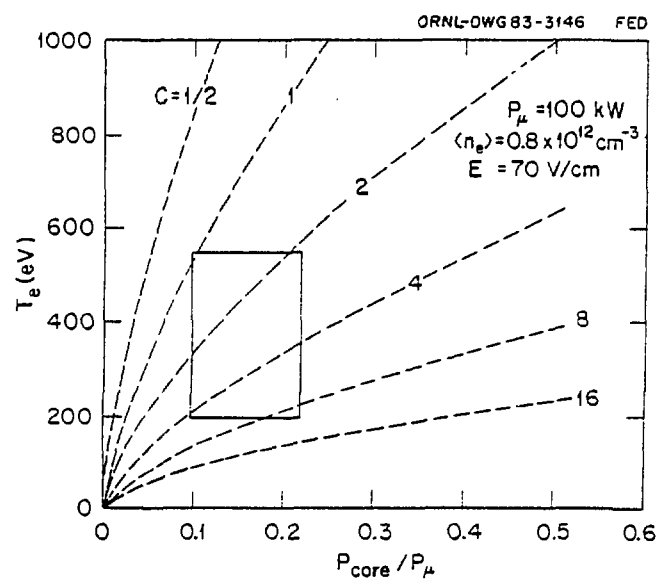

Fig. 20. Contours of constant ratio of theoretical neoclassical confinement time to experimentally measured energy confinement time are shown by the dashed curves as a function of T_e and P_{core}/P_μ. The area within our experimental uncertainties is shown by the rectangle.

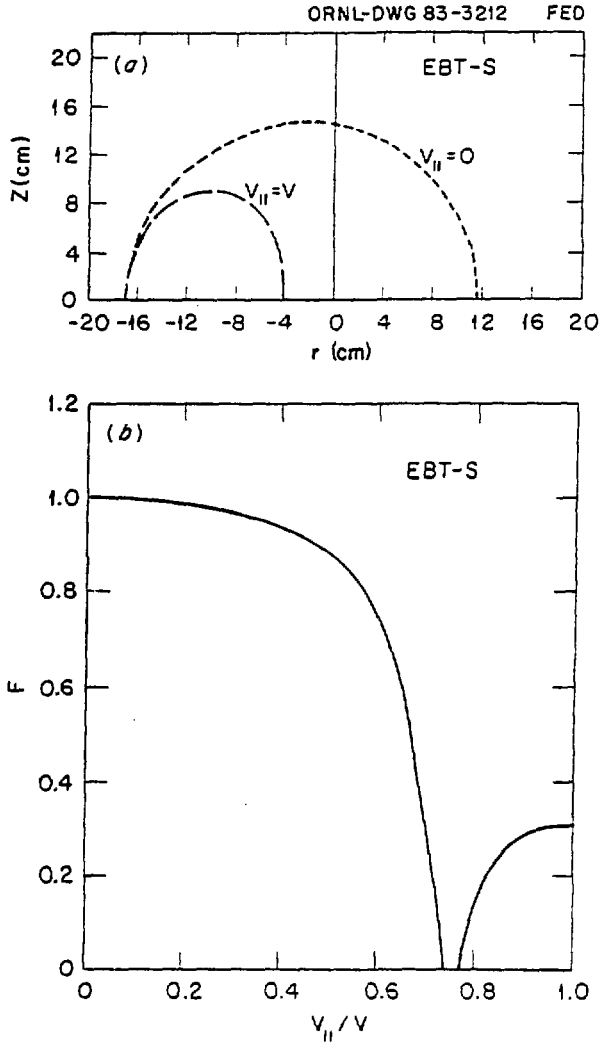

Fig. 21. EBT-S orbits. (a) $v_{||} = 0$ (i. e. fully trapped particles) dashed line, and $v_{||} = v$ (i.e. fully passing particles), solid line in a vertical cut through the torus midplane. (b) ratio of $F = A(v_{||}/v)/A(0)$ vs $v_{||}/v$, where F is the area of the maximum confined orbit relative to that of a completely trapped particle.

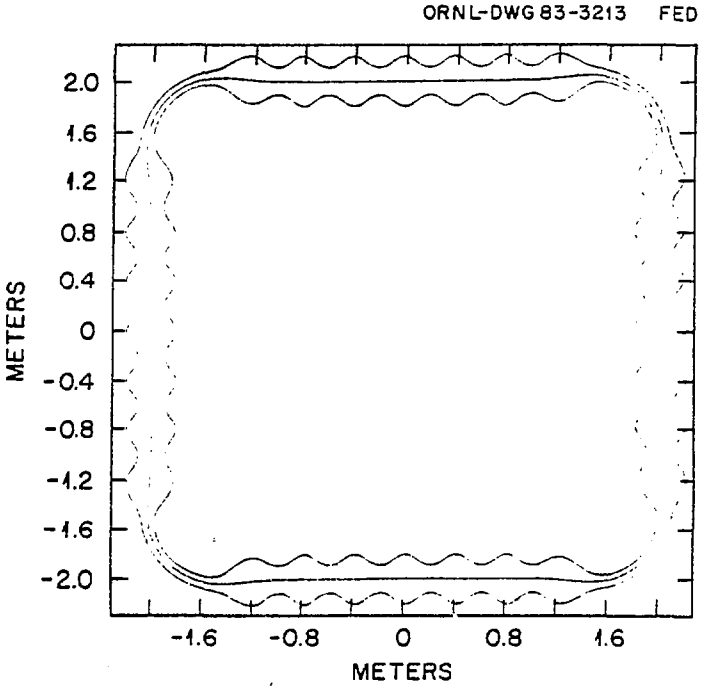

Fig. 22. Schematic plan view of EBS. Each of the four sides consists of six EBT-S coils.

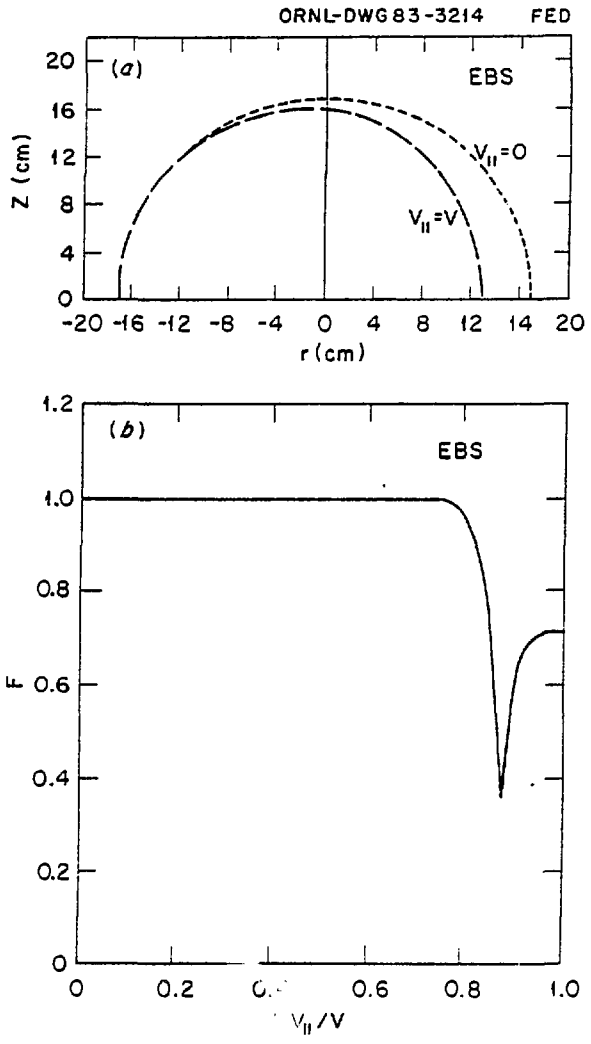

Fig. 23. Orbit calculations for EBS: (a) Orbits for $v_{\|} = 0$ and $v_{\|} = v$; (b) F vs $v_{\|}/v$.

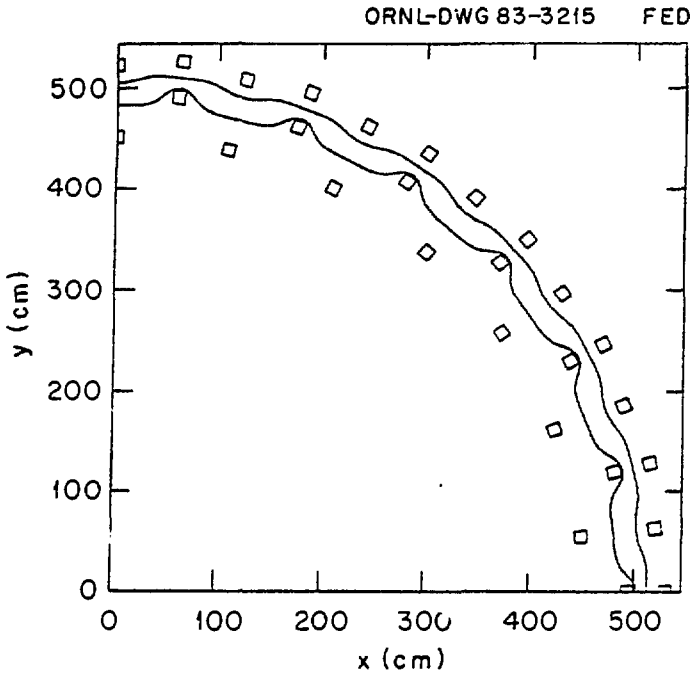

Fig. 24. Schematic plan view of one quadrant of an EBTEC design with R = 500 cm, with two magnetic lines of force shown.

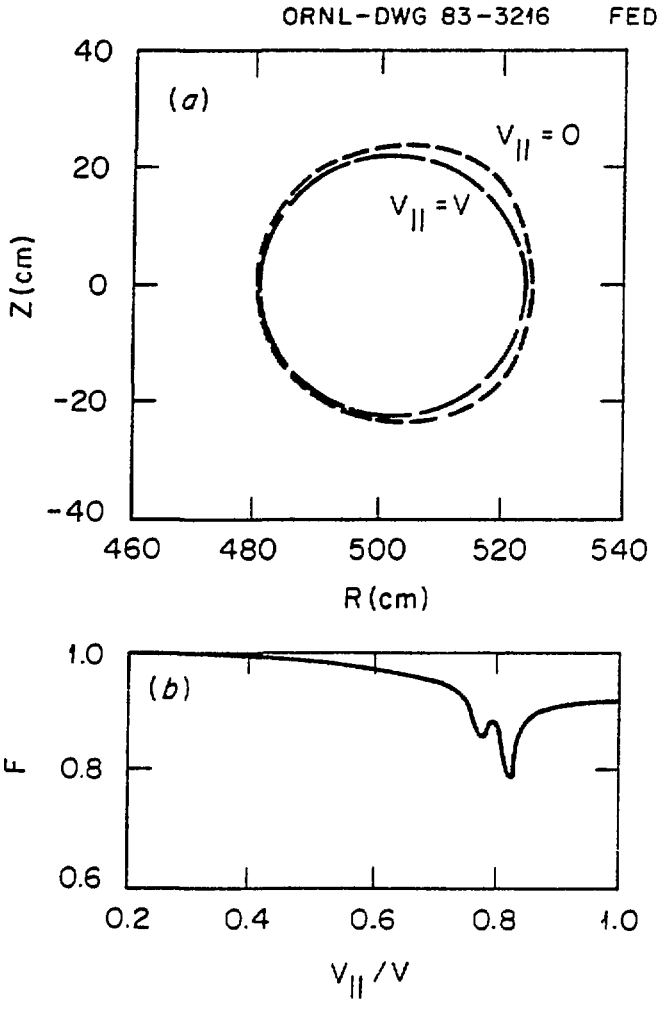

Fig. 25. (a) Orbits for EBTEC for $v_{\parallel} = 0$ and $v_{\parallel} = v$. (b) F vs $v_{\parallel}/v$ for EBTEC.

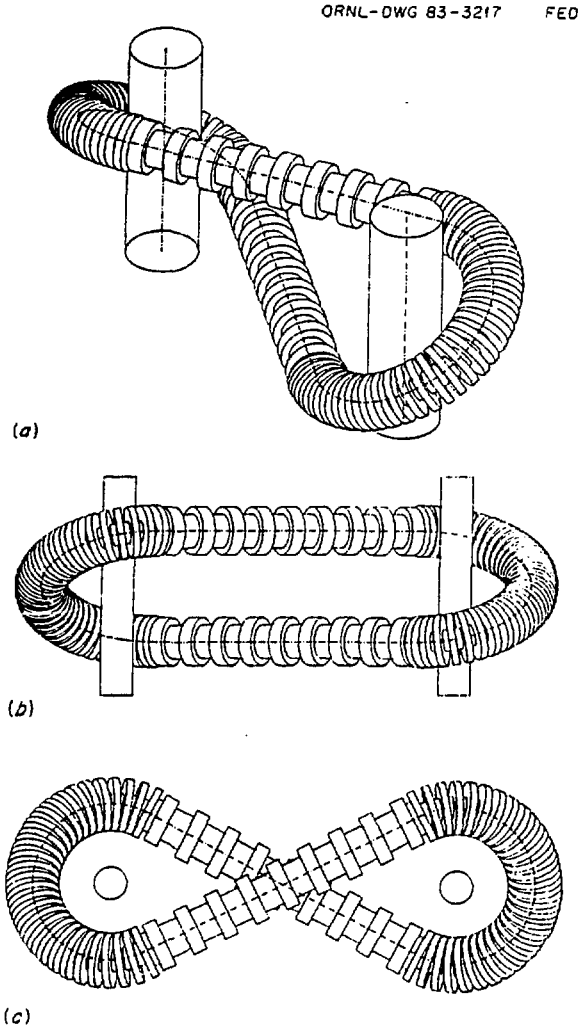

Fig. 26. Computer plots of three different views of the TRT device.

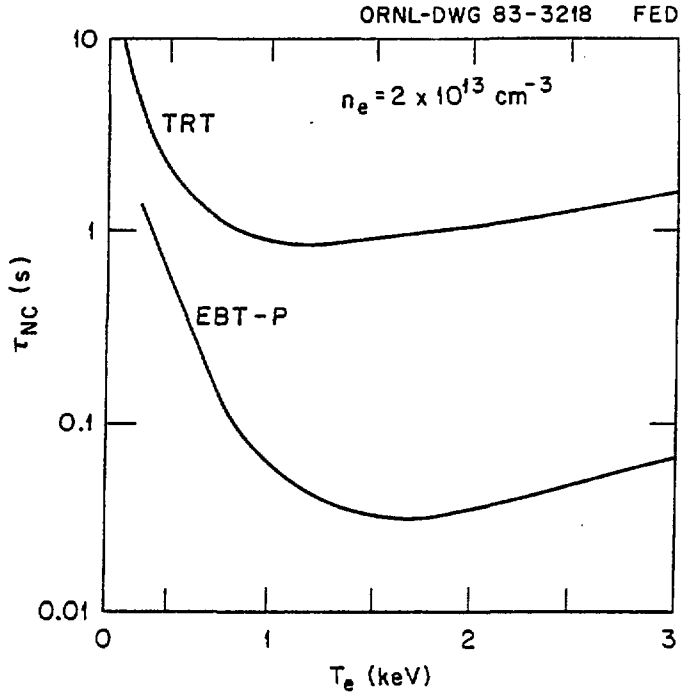

Fig. 27. Neoclassical particle confinement time (τ_{nc}) vs electron temperature for EBT-P and TRT. An electron density of 2×10^{13} cm^{-3} has been assumed.

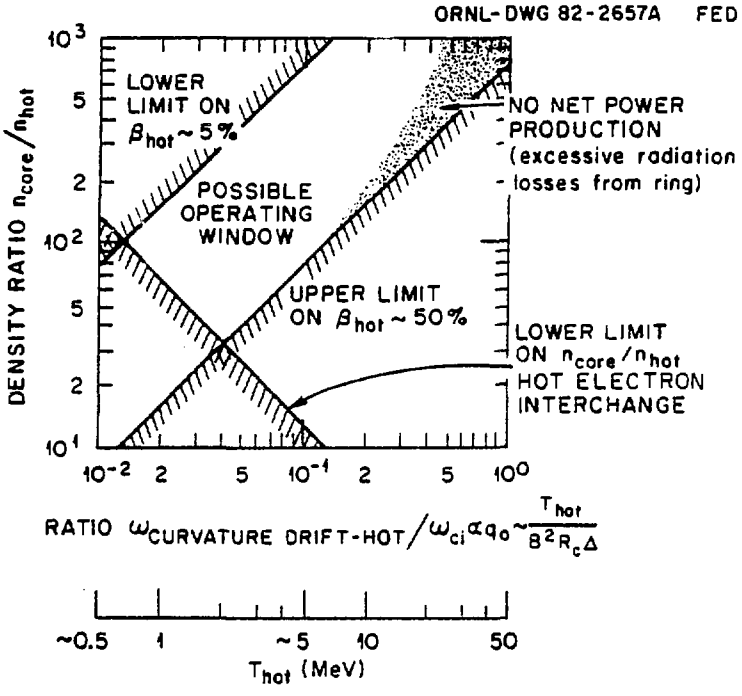

Fig. 28. Boundaries of a possible operating region for an EBT reactor vs n_{core}/n_{hot} and the ratio of the curvature drift frequency to the ion cyclotron frequency ($\sim T_{hot}$).

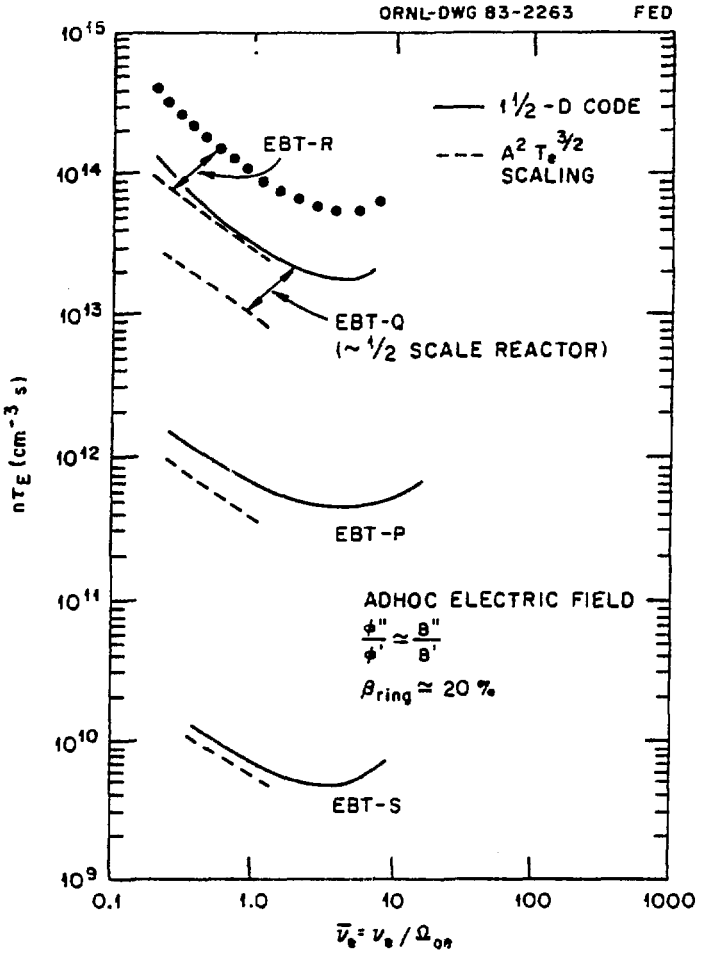

Fig. 29. The parameter $n\tau_E$ vs normalized collision frequency ν_e for four EBT devices. The dashed curves indicate 0-D scaling, while the solid or dotted curves include the effect of 1-D profiles. Curves are shown for the present device (EBT-S), for a prototypical reactor (EBT-R, see Table 3), and two devices (EBT-P and EBT-Q) of intermediate size.